Geophys. J. Int. (1994) **116,** 663–672

Source mechanism of the 1992 Roermond earthquake from surface-wave inversion of regional data

Jochen Braunmiller,* Torsten Dahm and Klaus-Peter Bonjer
Geophysikalisches Institut, Universität Karlsruhe, Hertzstrasse 16, 76187 *Karlsruhe, Germany*

Accepted 1993 July 29. Received 1993 July 28; in original form 1993 January 27

SUMMARY

The Dutch–German border region near the city of Roermond, The Netherlands was hit by a rather strong crustal earthquake at 1:20 UT, 1992 April 13. The epicentre is located within the Roer Valley Graben, a region currently undergoing extension. The centroidal source mechanism of this event has been retrieved by moment tensor inversion of broad-band long-period surface waves recorded at regional distances (100–1500 km). The double-couple contribution of the moment tensor corresponds to almost pure normal faulting (rake: 262°) on a steeply south-westward dipping fault (dip: 58°) with a NW–SE trend (strike: 138°). This result is consistent with local tectonics but violates some first-motion *P*-wave polarity data. The deduced seismic moment is 9.2×10^{16} N m corresponding to a moment magnitude of 5.3. A centroidal depth of 18 km fits slightly better than 13 km; however, the differences are small and other methods are necessary to constrain the depth further.

It is now possible to access a number of broad-band three-component seismic stations in Europe via phone line (e.g. German Regional Seismic Network) and the ORFEUS data centre (i.e. Global Digital Seismic Network). This allows retrieval of waveform data immediately after an earthquake. In this paper we present a potentially fast and reliable procedure for extracting the moment tensor from low-frequency surface waves using the Roermond earthquake as an example. Detailed knowledge of the velocity–depth structure along the travel paths seems unnecessary with our procedure. Further testing is required on all future moderate to strong earthquakes in Europe using rapidly accessible stations to investigate the procedure's usefulness and possible limitations as a tool for rapid moment tensor estimation.

Key words: moment tensor, regional waveforms, Roermond earthquake, source mechanism, surface-wave inversion.

1 INTRODUCTION

The Dutch–German border region experienced a strong earthquake in the early morning, 3:20 local time, of 1992 April 13. The epicentre (latitude: 51.17°, longitude: 5.93°, origin time: 1:20:02.7, Ahorner 1992) was located near Roermond within the NW–SE trending Roer Valley Graben in the south-eastern part of the Lower Rhine Embayment (Fig. 1). Damage in the epicentral region, especially in Roermond and nearby towns of Herkenbosch, The Netherlands and Heinsberg, Germany, is estimated at US$130–200 million (Berz 1992). However, no fatal building collapses occurred, and except for one death due to heart attack, no further casualties were reported (Ahorner 1992). A local magnitude of $M_L = 5.9$ and maximum intensity of VII was assigned (Ahorner 1992).

Hypocentral depths based on arrival-time data were determined by Ahorner (1992) and Paulssen, Dost & van Eck (1992) using HYPO71-program derivates. Ahorner (1992), who additionally used macroseismic observations, obtained a source depth of 14 ± 3 km, whereas Paulssen *et al.* (1992), using only NARS data, obtained 21 km. Paulssen *et al.* (1992) confirmed a source in the lower part of the upper crust by synthetic *P*-wave record sections. These best matched arrivals of later *P* phases in the NARS data set for a source depth of 20 ± 4 km.

The Lower Rhine Embayment is undergoing NE to SW

* Now at: College of Oceanic and Atmospheric Sciences, Oregon State University, Corvallis, OR 97331, USA.

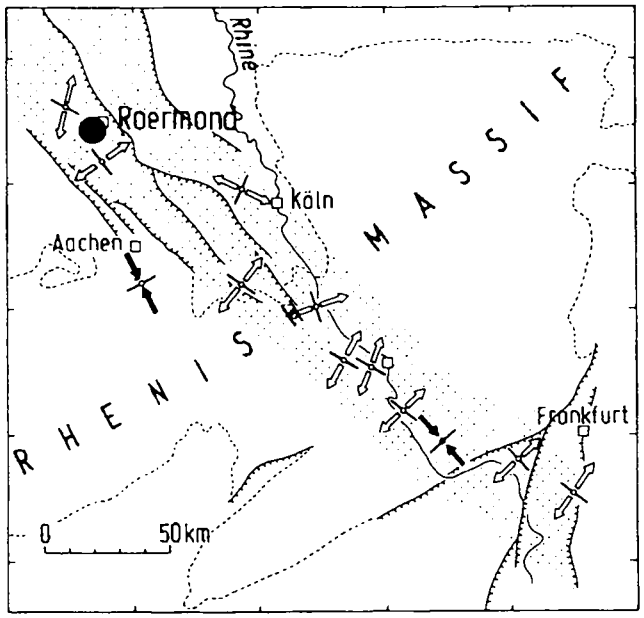

Figure 1. Map of the Lower Rhine Embayment and Rhenish Massif (modified after Ahorner 1983). The black circle shows the location of the epicentre near Roermond. The stippled area indicates extensional regime. The directions of white arrows indicate the horizontal projection of T-axes, while the directions of black arrows indicate the horizontal projection of P-axes. Tectonically active structures are marked by heavy lines with the down-thrown side hatched.

directed extension. The prevailing dislocation type derived from *P*-wave first-motion data is normal faulting (Ahorner, Baier & Bonjer 1983; Ahorner & Pelzing 1983; Ahorner 1983). Extension is also reflected by approximately 175 m relative vertical offset of Quaternary deposits at the eastern boundary fault—the so-called Peel Boundary fault—of the Roer Valley Graben (Ahorner 1983). The tectonic subsidence record derived from logs of exploration wells and shallow boreholes in the graben and its surroundings (Zijerveld *et al.* 1992) further confirms ongoing extension. Historical and present-day seismicity in this region is high compared to most other central European areas (Ahorner 1983). The last earthquake of similar strength, however, dates back to 1756. Therefore, the Roermond event is of great importance for earthquake hazard assessment procedures. In this paper, we concentrate on the source mechanism using broad-band surface waves.

Fault-plane solutions based on first-motion polarities indicating normal faulting were available within a few days of the event (Ahorner, private communication, 1992; Camelbeeck, private communication, 1992). With the recent installation of the German Regional Seismic Network (GRSN) and additional Global Digital Seismic Network (GDSN) data, it is now possible, within a few hours following an event, to obtain high-quality broad-band waveform data of European earthquakes at regional distances via phone line. Rapid determination of earthquake source parameters by inversion of regional broad-band body or surface waves has recently developed into an important topic in seismological research (e.g. Thio & Kanamori 1992; Wallace *et al.* 1992). The goal of this study is to demonstrate the feasibility of determining source parameters of moderate earthquakes in central Europe with immediately available waveform data using the Roermond earthquake as an example.

2 DATA AND METHOD

The GRSN currently consists of eight stations (Fig. 2) identically equipped with high-quality three-component broad-band STS-2 sensors and 24 bit high-dynamic range analogue-to-digital converters (Kind & Hanka 1992). Broad-band (80 samples s^{-1}), long period (1 sample s^{-1}), and decimated data streams can be retrieved (X.25 protocol) from all stations using the dial-up capability. We obtained broad-band data from the GDSN stations TOL and KONO through the GOPHER software from the ORFEUS data centre. Additional broad-band data from the stations STU and ETH, accessible via phone line (X.25 protocol), and from digital British stations were used to obtain a good azimuthal coverage (Fig. 2). Table 1 lists the stations used as well as their distances and azimuths from the epicentre. The instrument response was removed from the seismograms to obtain broad-band displacement records. A high-pass filter with cut-off at 100 s was applied to the data to avoid low-frequency instabilities.

The body-wave part of the observed seismograms at regional distances (100–1500 km) is rather complex and seems to be highly affected by heterogeneous crustal structures along different travel paths. Fig. 3 shows a record

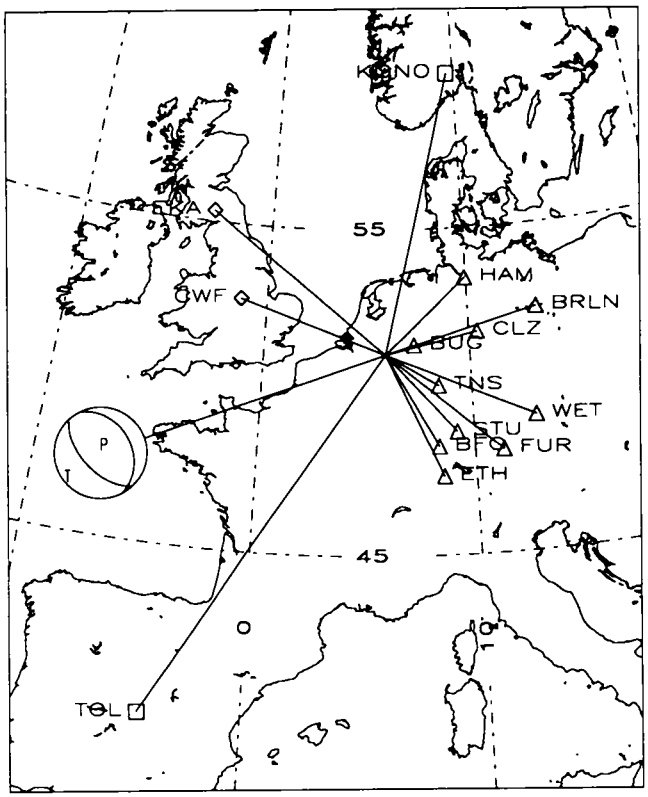

Figure 2. Map of western Europe. Great circle paths from the epicentre to stations used for surface-wave inversion are shown as straight lines. △: German Regional Seismic Network stations plus ETH and STU. □: Global Digital Seismic Network stations. ◇: British Geological Survey stations. The fault-plane solution shown corresponds to the double couple part of our inversion result.

Table 1. List of stations used in this study and their locations relative to the epicentre of the Roermond earthquake.

Station	Azimuth (°)	Distance (km)	INV	F3	F4
KONO	12	973	•		
HAM	45	376	•	•	•
BUG	71	100	•		
BRLN	72	533	•	•	•
CLZ	75	321	•	•	•
WET	111	547	•	•	•
TNS	120	206	•		
FUR	129	511	•	•	•
STU	137	356	•	•	•
BFO	150	360	•	•	•
ETH	155	458	•	•	•
TOL	215	1472	•		
BHM	273	330		•	
WOL	275	498		•	
HEA	275	500		•	
CWF	292	525	•	•	•
SCK	300	402		•	
EKA	311	761	•		

Azimuth: event-receiver azimuth. INV: '•' used for inversion; CWF, EKA-only vertical component, others: three components. F3: '•' shown in Fig. 3. F4: '•' shown in Fig. 4.

section of the *P*-wave displacements for stations at 300–600 km distance. Widths and amplitudes of the P_n-wavelets vary considerably. Attenuation of high-frequency signals differs significantly for different source–receiver paths (e.g. BRLN and WET). Stations located within the sedimentary basin of northern Germany, especially HAM, show large low-frequency oscillating signals.

The diversity of geological settings requires a detailed knowledge of the velocity–depth structure independent for each travel path in order to reliably retrieve source parameters from high-frequency body waves. We do not have this detailed knowledge for all travel paths. Furthermore, the necessity of a suitable velocity–depth structure for each source–receiver geometry would severely complicate a fast and standardized procedure for the retrieval of centroidal parameters. An unpursued approach could be to use simple crustal structures to model low-pass filtered P_{nl} waveforms (Helmberger & Engen 1980; Helmberger 1983).

Rather than using body waves, we concentrated on the internally more consistent lower frequency part of the surface waves (Fig. 4). Three-component data were available for all GRSN stations, GDSN stations, ETH and STU. We have only vertical component data from CWF and EKA. These were the only available British stations unclipped during the passage of the surface-wave group.

The excitation functions, representing the components of the synthetic seismograms, are calculated using the reflectivity method (e.g. Fuchs & Müller 1971; Müller 1985). Our simple model ($v_p = \sqrt{3} * v_s$) consists of a 30 km thick crust with $v_p = 6.0\,\mathrm{km\,s^{-1}}$, $Q_p = 400$, $Q_s = 300$, overlying a mantle with $v_p = 8.0\,\mathrm{km\,s^{-1}}$ at the Moho and a sub-Moho velocity gradient of 0.013 1/s, $Q_p = 500$, and $Q_s = 400$.

We used the extended version (Koch 1991a) of Sipkin's (1982) multichannel signal-enhancement moment tensor

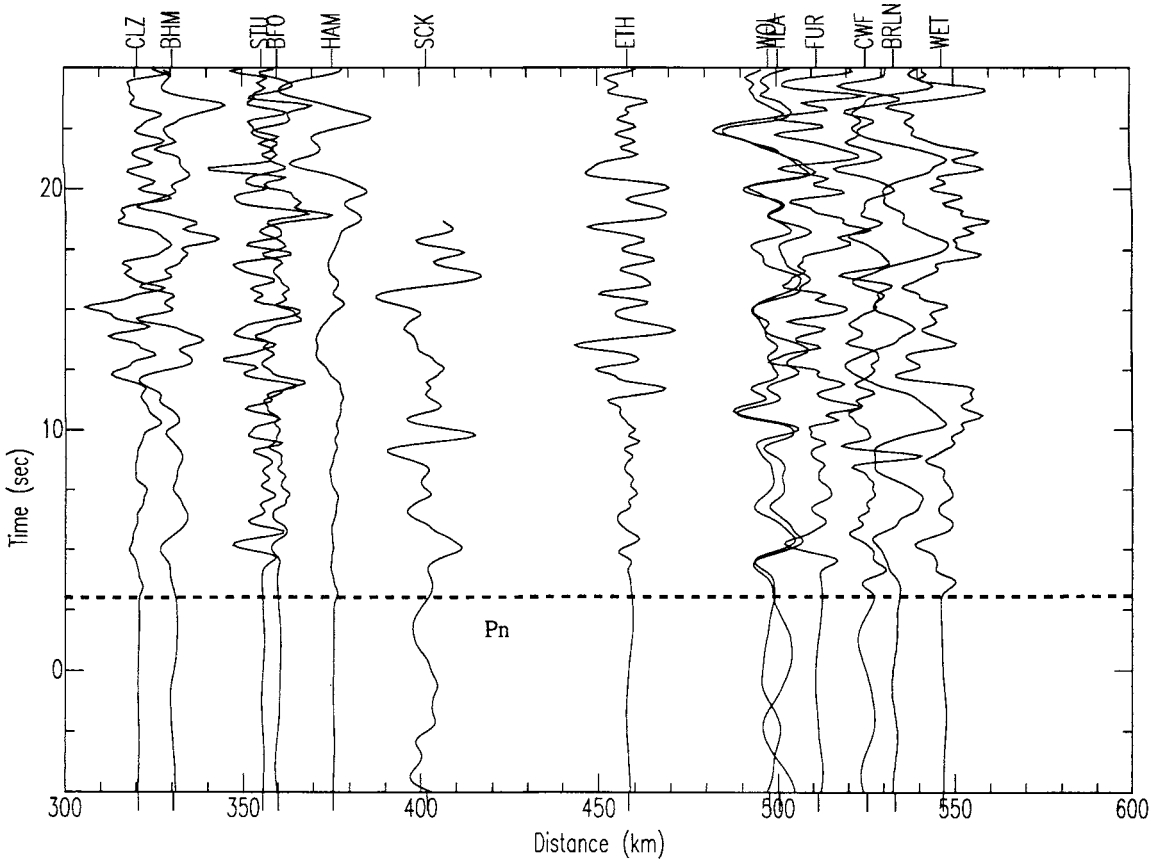

Figure 3. Observed *P*-wave displacement record section (normalized vertical component) in the distance range of 300–600 km. A reduction velocity of $7.8\,\mathrm{km\,s^{-1}}$ and a band-pass filter (0.04–2.5 Hz) has been applied. Station distances and azimuths are given in Table 1. The stippled line approximates the P_n onset and corresponds to a velocity of $7.8\,\mathrm{km\,s^{-1}}$. Zero on the time-scale corresponds to the event origin time.

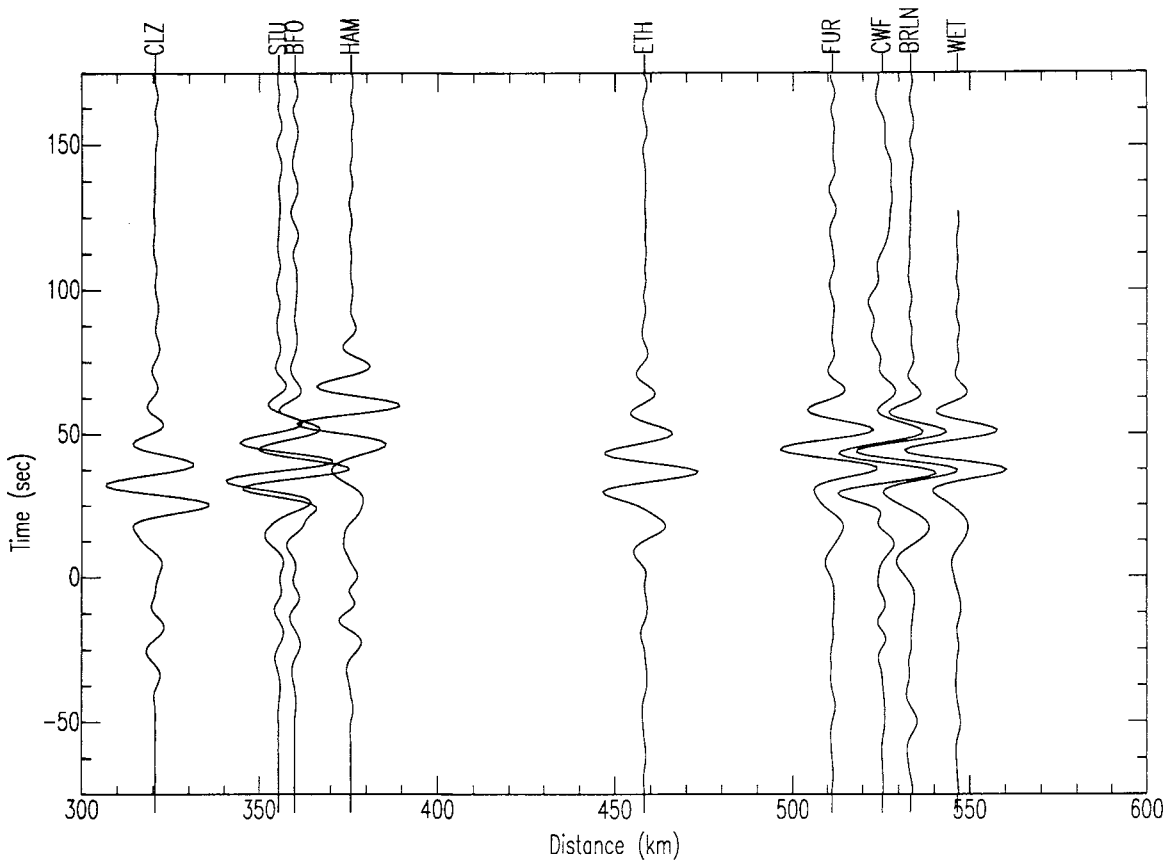

Figure 4. Observed surface-wave displacement record section (normalized vertical component) in the distance range of 300–600 km. A reduction velocity of 3.2 km s^{-1} and a band-pass filter (0.01–0.08 Hz) has been applied. Station distances and azimuths are given in Table 1. Zero on the time-scale corresponds to the event origin time. The CWF seismogram is flipped relative to the other seismograms. The coherence between different stations, even for different azimuths, is striking. Only the wave train at HAM arrives much later, which is probably caused by local travel path effects.

inversion to recover the moment tensor components of a point source in space and time, and obtained the centroidal (average) source description. The time-domain inversion for the six independent moment tensor components is linear and minimizes the least-squares norm between observed and synthetic seismograms. This inversion method has been applied to local (Koch 1991b) and routinely to teleseismic (Spikin 1986; Sipkin & Needham 1993) body-wave data, while we apply it to surface waves observed at regional distances. Previously, source parameter inversions of regional surface-wave data were successfully performed in the spectral domain using regionalized propagation path corrections (e.g. Patton 1982; Beck & Patton 1991).

For the moment tensor inversion, we used periods of 12.5 s to 100 s with the main contributions having a period of about 20 s corresponding to a 50–70 km wavelength. Our simple velocity–depth model does not account for the correct traveltimes. Since we expect a biased solution when the observed seismograms and synthetic Green's functions are not correctly aligned, we applied an iterative procedure to account for this bias. First, we inverted for the moment tensor while synthetic Green's functions and observed data were not shifted relative to each other. Then synthetic seismograms were constructed from the moment tensor and the Green's functions. We displayed synthetic and observed seismograms, and interactively shifted the synthetics such that corresponding phases were aligned. For each station the vertical and radial components, corresponding to the Rayleigh wave contribution, were always shifted by the same amount. With the shifted Green's functions the moment tensor inversion was repeated. The new solution should be less biased since traveltime corrections were applied individually for each station. Further refinements can be obtained by repeating the shifting and inversion loop. The basic requirement for this procedure to work is that the traveltime errors introduced by the velocity–depth structure are smaller than about one-fourth of the wave period. This implies that the initial moment tensor estimate obtained before realigning is biased but not grossly incorrect. In our case the dominant wave period in the bandpass filtered observed seismograms was about 20 s (Fig. 4) and the shift of the synthetic (except for stations KONO, HAM and EKA) with respect to the observed data for our final result (Table 2) was only up to ±3 s for individual traces in agreement with the above requirements.

In the multichannel signal enhancement method the quality of the fit between synthetic seismograms and observed data, and the overall goodness of the parameter estimates are described by the normalized-mean-square error (NMSE) (e.g. Table 2). However, formal statistical error bounds for individual moment tensor components are difficult to obtain with this method (Sipkin 1982). We

Table 2. Source parameters of the Roermond earthquake. First two rows this study, rows 3–5 other studies (see below).

Depth (km)	Strike (°)	Dip (°)	Rake (°)	M_o (10^{16} Nm)	I/D (%)	DC (%)	NMSE	Ref.
13*	139±2	58±1	263±2	9.4±0.5	23	89	0.44	TS
18*	138±2	58±1	262±2	9.2±0.4	15	95	0.43	TS
14†	124†	68†	270†	6.5†				A
20†	124†	70†	270†					P
15*	143	68	273	13.3	0	86		CMT

Depth: centroid depth. Strike, Dip, Rake: following convention of Aki & Richards (1980). M_o: seismic moment. I/D: ratio of isotropic to largest deviatoric eigenvalue of moment tensor. DC: double-couple component of deviatoric part, $1-2\cdot\varepsilon$, ε is the ratio of the smallest to largest deviatoric eigenvalue of moment tensor (following Dziewonski *et al.*, 1981). NMSE: normalized mean square error (following Sipkin, 1982). Ref.: reference; TS: this study; A: Ahorner (1992); P: Paulssen *et al.* (1992); CMT: Dziewonski *et al.* (1993). Uncertainties following strike, dip, rake, and M_o are two standard deviations computed using a jack-knife and bootstrap procedure. †: see text for details. *: fixed during inversion.

obtained formal error estimates using resampling techniques. Resampling methods like jack-knifing and bootstrapping are convenient but computationally intensive methods for the estimation of standard errors for any statistic. Tichelaar & Ruff (1989) provide a short 'hands-on' introduction. For more details, Efron (1982) and Efron & Tibshirani (1986) are recommended. We apply a two-step procedure. First a 'delete-1' jack-knife is used to estimate the moment tensor components and their standard errors. Then a bootstrap with 200 bootstrap samples is applied to estimate the orientation and standard errors of the double couple. The sample size of 200 is based on examples presented in Efron & Tibshirani (1986). As shown in Efron & Tibshirani (1986), jack-knife and bootstrap methods provide conservative statistical error estimates.

3 RESULTS

The results of the moment tensor inversion are summarized in Table 2. Table 3 shows the complete moment tensor for centroid depths of 13 km and 18 km. The fit of the synthetic seismograms for a source depth of 18 km is shown in Fig. 5.

Table 3. Moment tensors from surface-wave inversion.

Depth (km)	M_{xx}	M_{xy}	M_{xz}	M_{yy}	M_{yz}	M_{zz}	M_o (10^{16} Nm)
13*	.08	.39	-.34	.38	-.27	-1.16	9.4
	.07	.03	.02	.07	.02	.03	0.5
18*	.42	.45	-.33	.77	-.27	-.73	9.2
	.09	.04	.02	.08	.02	.03	0.4

Depth: centroid depth. M_{ij}: moment tensor components. M_o: seismic moment. The uncertainties given below each component and M_o are two standard deviations computed using a 'delete-1' jack-knife procedure. *: fixed during inversion.

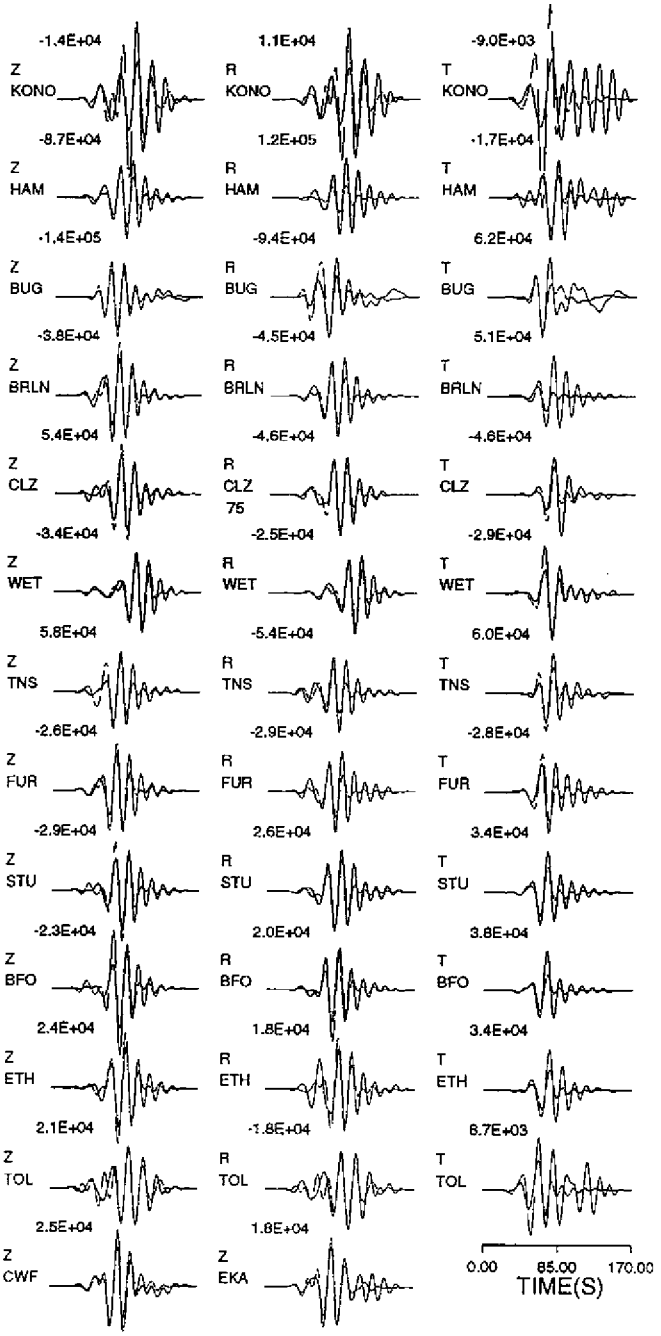

Figure 5. Fit of the synthetic seismograms (dashed) to the observed displacement seismograms (solid) for a source depth of 18 km. The inversion window is 170 s long. The seismograms are normalized with respect to the maximum observed amplitude, which is shown above each trace (in nm). The first column shows the vertical (Z), the second the radial (R), and the third the transverse component (T). The last row shows the vertical (Z) component of the two British stations. The stations are ordered azimuthally.

One nodal plane (Table 2) corresponds to a steeply south-westward dipping ($58° \pm 1°$) and NW–SE striking ($138° \pm 2°$) normal fault (rake: $262° \pm 2°$). Many of the aftershocks recorded by a temporal network align along this steeply dipping plane (Camelbeeck, private communication, 1992) constraining the fault plane. Predominant normal faulting is consistent with the surface tectonics of the region.

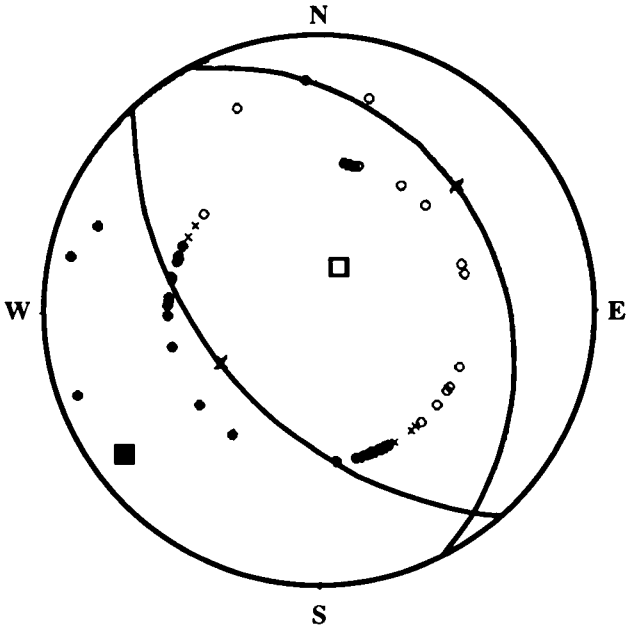

Figure 6. Lower hemisphere equal-area projection of *P*-wave first-motion polarity data. ●, Compressional arrivals; ○, dilatational arrivals; ×, nodal arrivals. The data were read by the authors. The focal mechanism shown corresponds to the double-couple part of our inversion result. ■, T-axis; □, P-axis. The first-motion data require a steeper dip, which may indicate a change in focal mechanism by about 10° between rupture onset and centroid.

The isotropic source part (I/D in Table 2) is small, and the double-couple component (DC in Table 2) dominates the deviatoric part for both source depths. (For an explanation of 'I/D' and 'DC' see the footnote to Table 2). This is consistent with shear failure along a fault. The seismic moment of $(9.2 \pm 0.4) \times 10^{16}$ Nm corresponds to a moment magnitude of $M_w = 5.3$, which is considerably smaller than the estimated local magnitude of $M_L = 5.9$ (Ahorner 1992).

The first motion *P*-wave polarity data (Fig. 6) we compiled failed to constrain the second nodal plane. Some first-motion data requiring a steeper dip (stations in the south-east and west), seem to contradict the waveform inversion result. A small change in focal mechanism, about 10°, between the rupture onset (represented by the first-motion data) and the centroid, could explain the discrepancy.

The best-fitting centroid depth was found by grid search. In the first set of inversions no constraint was imposed on the moment tensor. Fig. 7(a) shows both the misfit (NMSE) as a function of centroid depth and the isotropic (I/D) and double-couple (DC) contributions of the moment tensor. In the second set of inversions a deviatoric constraint (i.e. no isotropic-source contribution, I/D = 0 per cent) was applied. Fig. 7(b) shows the misfit and the double-couple contribution. In both cases (Figs 7a and b) the misfit has a minimum at 18 km centroid depth. Furthermore, the non-double-couple contributions (combination of I/D and 100 per cent-DC) indicating possible deviations from a pure shear failure are smallest for 18 km depth. Non-double couple contributions may therefore be a result of fitting non-source related, unmodelled crustal effects, artificially

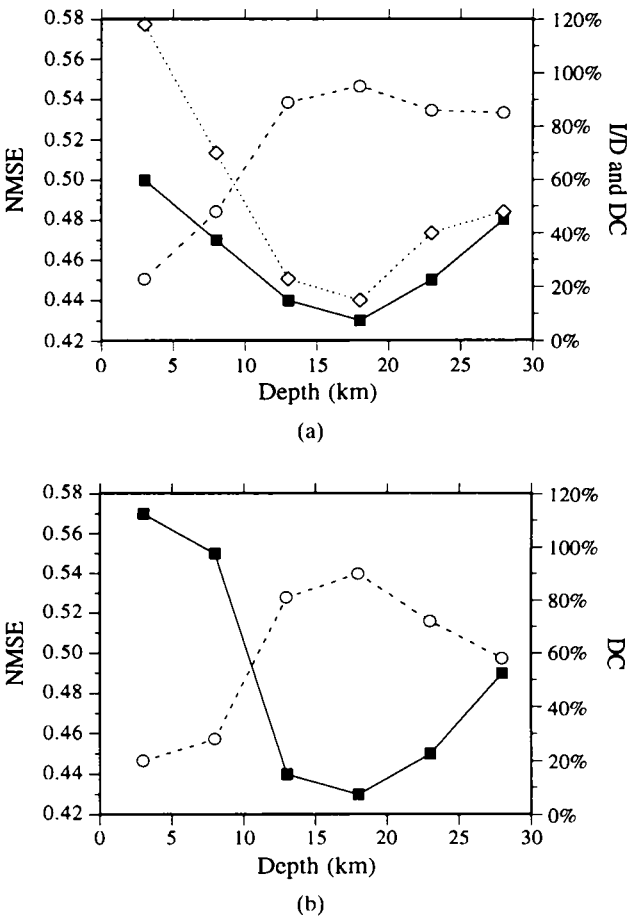

Figure 7. (a) Normalized mean-square error (■, NMSE) and non-double-couple parts of the moment tensor (◇, I/D; ○, DC) versus centroid depth for unconstrained inversion. For an explanation of 'I/D' and 'DC', see Table 2. (b) Same as for (a) but deviatoric constraint applied ($M_{xx} + M_{yy} + M_{zz} = 0$, I/D = 0 per cent).

improving the misfit. The double-couple mechanism and seismic moment for source depths from 8 km to 23 km remain very stable for both the unconstrained and the constrained inversion.

4 RESOLUTION

We applied several tests to investigate the resolving power of our procedure. One important factor limiting the resolution of the source parameters are the amplitudes and shapes of the Green's functions which depend on centroid depth and epicentral distance. In a radially symmetric Earth (velocity varies only with depth) each component of the displacement field can be described as a combination of moment tensor components, aximuth-dependent terms, and three excitation functions for *P–SV* waves or two excitation functions for *SH* waves (Ward 1980; see e.g. Nábelek 1984; Dahm 1992).

Figure 8 shows the vertical and transverse excitation functions E^2, E^1 and (only for the vertical component) E^0 calculated with our simple velocity–depth model for an epicentral distance of 320 km and centroid depths of 3 km,

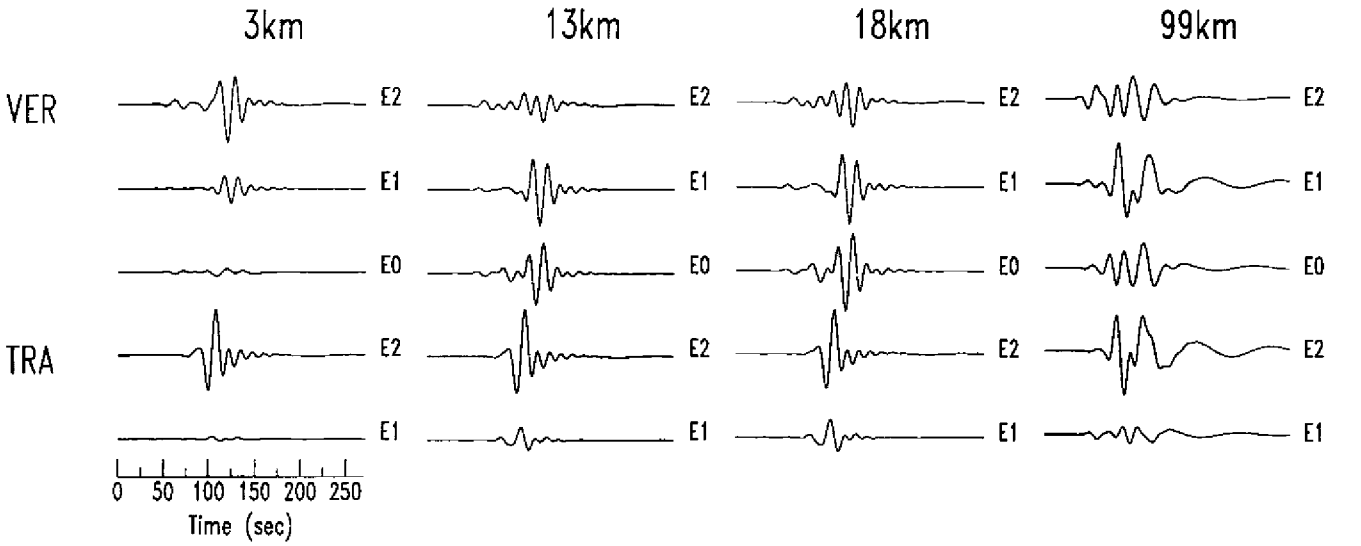

Figure 8. Vertical and transverse excitation functions E^2, E^1, and E^0 (vertical only) for an epicentral distance of 320 km and centroid depths of 3 km, 13 km, 18 km and 99 km. The excitation functions are the responses to a unit-step source. The traces are normalized to the largest excitation function in each column, the transverse E^2. The amplitude ratio of the transverse E^2 functions is 100:87:76:8 for depths of 3, 13, 18 and 99 km.

13 km, 18 km and 99 km. The strike-slip part of the source excites E^2. The horizontal thrust or vertical dip-slip part depends on the E^1 excitation function. The M_{zz} component of the moment tensor, which represents a vertical force dipole, depends on $2E^0 - E^0$ or respectively on E^2. A good resolution of the individual source components is possible if all excitation functions are non-zero, approximately equal in amplitude, and different in shape.

The strike-slip part is well resolved when the Love waves are included. E^0 becomes very small for shallow sources. However, $2E^0 - E^2$ is always of significant amplitude, and the M_{zz} component should be well resolved. Due to the stress-free boundary condition at the Earth's surface, the excitation functions E^1 vanish for Love and Rayleigh waves. This is apparent from the relatively small amplitudes of the E^1 excitation functions (Fig. 8) for a centroid depth of 3 km. Therefore, for shallow sources and long-period data, the horizontal thrust or vertical dip-slip part of the moment tensor is usually the least resolved (e.g. see also Fig. 2 of Dziewonski, Chou & Woodhouse 1981). The shapes and amplitudes of the excitation functions for sources at 13 km and 18 km depth are quite similar, explaining why the centroid depth is not very well resolved. However, all moment tensor components are well resolved for crustal earthquakes below a few kilometres source depth, and no additional constraints are necessary for their retrieval. A better resolution of the centroid depth could be obtained using higher frequencies in our analysis method. Including higher frequencies would probably be necessary to analyse smaller events ($M \approx 4$–5), but would require the implementation of a finer, more accurate, velocity–depth model.

Azimuthal station coverage is another important factor limiting the resolution of source parameters. For earthquakes occurring in certain regions of Europe, the azimuthal station coverage may degrade significantly. We tested the stability of the inversion by excluding the British and the GDSN stations. The remaining stations (GRSN, STU and ETH) cover only an azimuthal sector of 110° and are all located east of the source, but the inversion results did not change significantly. For an 18 km centroid depth we obtained a source orientation of $136 \pm 3°/57 \pm 1°/260 \pm 2°$ for strike, dip and rake, and a seismic moment estimate of $(11.3 \pm 0.6) \times 10^{16}$ N m (compare with results in Table 2). The stability of these results indicates that our procedure, even in the case of an unfavourable station distribution, allowed a reliable recovery of the moment tensor provided three-component data are available. Additional dial-up-access (PSZ in Hungary is already accessible, and in the near future there will be four more GRSN stations in the northern and eastern part of Germany) and inclusion of more stations to the ORFEUS data centre (DPC in Czechoslovakia is already included) will improve the station coverage of rapidly accessible stations.

Correct alignments of the synthetic data with respect to the observed seismograms are crucial to our procedure. For an 18 km centroid depth we investigated the effects caused by systematic misalignments and by random misalignments. First we shifted all synthetic data such that they were 3 s, 2 s, 1 s early and 1 s, 2 s, 3 s late, relative to the best-fitting alignments. Introducing these systematic misalignments caused considerable increase in the NMSE misfit (Fig. 9). For misalignments of either plus or minus 1 s, which is probably the accuracy of our alignments, the source orientation changed by ±5° in strike, ±6° in dip, and ±10° in rake relative to the solution in Table 2. Next we investigated the effects of random changes in alignments up to ±2 s for individual traces relative to the best-fitting alignments. 30 models were generated. All fit considerably worse than the best alignments (NMSE: 0.47–0.60 compared to 0.43 for best fit). The source orientation was contained within the following bounds: strike: 129°–145°; dip: 47°–66°; rake: 251°–269°. The average of the 10 best models was: 140°/58°/263° for strike, dip and rake—very similar to our best fit. We did not cover the complete solution space, but these tests may outline the stability properties of our inversion procedure.

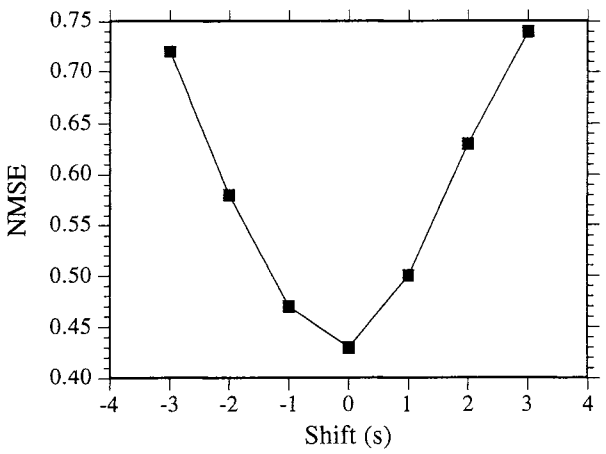

Figure 9. Normalized mean-square error (NMSE) as a function of systematic misalignment. Negative shifts mean that all synthetics are too early, and positive shifts that all synthetics are too late relative to the best-fitting alignments.

5 DISCUSSION

5.1 Source parameters

The orientation of the nodal planes determined from surface-wave inversion (Table 2) differ by about 10° in strike, dip and rake from the first-motion fault-plane solution of Ahorner (1992). Forward modelling of the *P*-wave group by Paulssen *et al.* (1992) using data from the Dutch NARS array resulted in a solution almost identical to Ahorner's (see Table 2). Most NARS stations are located about 50–200 km north and north-east of the epicentre. Synthetic and observed record sections were compared by eye to find the best-fitting source orientation. Changing the orientation by more than 10° from their preferred solution significantly degraded the fit (Paulssen *et al.* 1992). The centroid-moment tensor (CMT) solution of Dziewonski, Ekström & Salganik (1993) deduced from teleseismically recorded long-period body waves is also consistent with our solution (see Table 2). During their inversion the centroid depth was fixed to 15 km based on constraints from broad-band body waves. The most severe difference between our and other published results is our 10° shallowing of the dip angle. The uncertainty in our dip estimate, including effects due to misalignments and incorrect crustal structure, is probably on the order of 10°. However, very steeply (or very shallowly) dipping normal faulting earthquakes, like suggested for the Roermond earthquake by a dip angle of 68°–70° (Ahorner 1992; Paulssen *et al.* 1992; Dziewonski *et al.* 1993), are rarely observed world-wide (e.g. Doser & Smith 1989; Jackson & White 1989).

Our seismic moment estimate, $(9.2 \pm 0.4) \times 10^{16}$ N m, corresponding to a moment magnitude of $M_w = 5.3$, depends on the crustal structure. As shown in the previous section, excluding the British and GDSN stations increased the seismic moment estimate by about 20 per cent. This effect may be caused by insufficiencies in the Q-values of our simple velocity–depth model, since these stations are located farther away from the epicentre than the other stations. The Q-values of our original model are at the higher end of possible values (e.g. Anderson & Given 1982), therefore we probably underestimate the seismic moment slightly. Changing the Q-values affects the seismic moment estimates but not the source orientation. Assuming Q is one-half and one-fourth of the original values resulted in moment estimates of $(10.1 \pm 0.5) \times 10^{16}$ N m and $(13.1 \pm 0.6) \times 10^{16}$ N m, respectively. Our estimate is consistent with the CMT result of 13.3×10^{16} N m ($M_w = 5.4$) (Dziewonski *et al.* 1993) and estimates based on body-wave spectra. From the *P*-wave spectrum at BNS ($\Delta = 92$ km) Ahorner (1992) obtained $M_o = 6.5 \times 10^{16}$ N m. The average estimate from *P* and *SH* waves for BUG ($\Delta = 100$ km) was $M_o = 8.3 \times 10^{16}$ N m (Oncescu, private communication, 1992). On the other hand, local magnitude (M_L) estimates of 5.8 (Camelbeeck, private communication, 1992) to 5.9 (Ahorner 1992) were considerably higher. Scherbaum (1993) simulated strong ground-motion data consistent with maximum observed accelerations, *P*- and *S*-wave spectra at BUG, and local magnitude estimates. Scherbaum (1993) obtained a moment estimate of $(23–36) \times 10^{16}$ N m (M_w = 5.5–5.7) for a source depth of 21 km. However, the relatively (with respect to $M_L = 5.8–5.9$ estimates) minor damage in the epicentral region and the relatively small accelerations measured (Ahorner 1992) may be related to a low seismic moment release consistent with our estimate.

The centroidal depth was not tightly constrained by our long-period surface-wave inversion (Fig. 7). Additional uncertainties in the depth estimate were probably introduced by our crustal model. For our simple layer over half-space model an 18 km centroid depth fits slightly better than 13 km. Other methods are required to better constrain the depth.

5.2 Potential applications

For relatively moderate earthquakes (about $4.0 \leq M_w \leq 6.0$), the simple and potentially fast procedure presented here could be a useful augment to the CMT method, which already provides moment tensor solutions of large earthquakes available within hours following an event. In contrast to the CMT method (see Dziewonski *et al.* 1981; Dziewonski & Woodhouse 1983), we utilized only surface waves which have the largest amplitudes. CMTs use teleseismic data, while our data were recorded at regional distances ($\Delta \approx 100–1500$ km). We inverted for the seismic moment tensor but not for centroid location in space and time. As described, data up to a 12.5 s period are presently included. This allowed reliable unconstrained inversion for all moment tensor components even for relatively shallow sources.

More earthquakes must be studied in order to examine the reliability of the method, the dependance on the crustal model, and the influence of errors introduced by incorrect seismogram alignments. Finding the magnitude bounds within which the source mechanism can be reliably retrieved will be important.

6 CONCLUSIONS

In agreement with other studies (Ahorner 1992; Paulssen *et al.* 1992; Dziewonski *et al.* 1993), we found from surface-wave inversion that the average source mechanism of the Roermond earthquake represents almost pure normal

faulting on a steeply south-westward dipping fault. The strike obtained from surface-wave inversion is compatible with the NW–SE trend of the Roer Valley Graben. The estimated seismic moment corresponds to a moment magnitude of 5.3, which is considerably smaller than the estimated local magnitudes (Camelbeeck, private communication, 1992; Ahorner 1992).

Using the long-period surface-wave data we were not able to resolve details of the rupture process (e.g. the source–time history), since the source becomes point-like in space and time for low-frequency observations. Furthermore, the excitation functions are not sensitive to small variations in the centroid depth—a centroid depth of 18 km fits only slightly better than 13 km.

Waveform data from the GRSN and GDSN nets can be obtained within hours of an earthquake. They are high quality, high dynamic range, broad-band records. Even a simple velocity–depth model is sufficient to obtain a reliable centroidal moment tensor solution when the long-period surface wave part of the seismograms are used, and synthetic and observed seismograms are interactively aligned. The procedure presented here is potentially fast and should be tested on moderate earthquakes at regional distances within Europe.

ACKNOWLEDGMENTS

B. Dost of the ORFEUS data centre kindly provided data from the GDSN and BGS stations. W. Friederich made available to us data of the stations ETH, STU and WET. H. Paulssen sent us a preprint of their paper. E. Wielandt, W. Zürn and G. Laske helped to clarify instrument responses of the GRSN stations. R. Widmer made the jack-knife and bootstrap procedures for error analysis available to us. Fig. 6 was plotted using a code written by M. C. Oncescu. Thanks to M. C. Oncescu and T. Camelbeeck for sharing their results before publication. Thanks go to the station and network operators for supplying us with the necessary station information and the seismogram copies. Reviews by W. Brüstle, K. Koch and an anonymous reviewer helped considerably to clarify and improve the manuscript. JB wishes to thank John Nábelek for support during the final stages of this paper. This research has been supported through the CEC Transfrontier project, the SFB 108 of the German science foundation, and the IDNDR project of the University of Karlsruhe.

REFERENCES

Ahorner, L., 1983. Historical seismicity and present-day microearthquake activity of the Rhenish Massif, Central Europe, in *Plateau Uplift—The Rhenish Massif, A Case History,* pp. 198–221, eds Fuchs, K., von Gehlen, K., Mälzer, H., Murawski, H. & Semmel, A., Springer, Berlin.

Ahorner, L., 1992. Das Erdbeben bei Roermond am 13. April 1992 und die daraus zu ziehenden Lehren für das Erdbebengefährdungspotential im Rheinland (in German), *DGG Mitteilungen,* **1–2,** 51–57.

Ahorner, L. & Pelzing, R., 1983. Seismotektonische Herdparameter von digital registrierten Erdbeben der Jahre 1981 und 1982 in der westlichen Niederrheinischen Bucht (in German), *Geol. Jb.,* **E26,** 35–63.

Ahorner, L., Baier, B. & Bonjer, K.-P., 1983. General pattern of seismotectonic dislocations and the earthquake-generating stress field in Central Europe between the Alps and the North Sea, in *Plateau Uplift—The Rhenish Massif, A Case History,* pp. 187–197, eds Fuchs, K., von Gehlen, K., Mälzer, H., Murawski, H. & Semmel, A., Springer, Berlin.

Aki, K. & Richards, P.G., 1980. *Quantiative Seismology,* Freeman, San Francisco.

Anderson, D.L. & Given, J.W., 1982. Absorption band Q model for the Earth, *J. geophys. Res.,* **87,** 3893–3904.

Beck, S.L. & Patton, H.J., 1991. Inversion of regional surface-wave spectra for source parameters of aftershocks from the Loma Prieta earthquake, *Bull. seism. Soc. Am.,* **81,** 1726–1736.

Berz, G., 1992. Roermond-Beben: Schäden in Höhe von 200–300 Millionen DM (in German), *Naturkatastrophen, Nachrichten a. d. deutschen Kommittee der int. Dekade f. Katastrophenvorbeugung (IDNDR),* **4/92,** 3–6.

Dahm, T., 1992. Seismic moment tensor decomposition and the resolution of elementary sources for small earthquakes, *SFB 108 Berichtsband 1990–1992,* 943–958.

Doser, D.I. & Smith, R.B., 1989. An assessment of source parameters of earthquakes in the Cordillera of the western United States, *Bull. seism. Soc. Am.,* **79,** 1383–1409.

Dziewonski, A.M. & Woodhouse, J.H., 1983. An experiment in systematic study of global seismicity: centroid-moment tensor solutions for 201 moderate and large earthquakes of 1981, *J. geophys. Res.,* **88,** 3247–3271.

Dziewonski, A.M., Chou, T.-A. & Woodhouse, J.H., 1981. Determination of earthquake source parameters from waveform data for studies of global and regional seismicity, *J. geophys. Res.,* **86,** 2825–2852.

Dziewonski, A.M., Ekström, G. & Salganik, M., 1993. Centroid-moment tensor solutions for April–June 1992, *Phys. Earth planet. Inter.,* **77,** 151–163.

Efron, B., 1982. The jackknife, the bootstrap, and other resampling plans, *Soc. Ind. Appl. Math. CBMS-Natl. Sci. Found. Monogr.,* **38**.

Efron, B. & Tibshirani, R., 1986. Bootstrap methods for standard errors, confidence intervals, and other measures of statistical accuracy, *Stat. Sci.,* **1,** 54–77.

Fuchs, K. & Müller, G., 1971. Computation of synthetic seismograms with the reflectivity method and comparison with observations, *Geophys. J. R. astr. Soc.,* **23,** 417–423.

Helmberger, D.V., 1983. Theory and application of synthetic seismograms, in *Earthquakes: Observations, Theory and Interpretation,* pp. 174–222, eds Kanamori, H. & Boschi, E., North-Holland, Amsterdam.

Helmberger, D.V. & Engen, G.R., 1980. Modeling the long-period body waves from shallow earthquakes at regional ranges, *Bull. seism. Soc. Am.,* **70,** 1699–1714.

Jackson, J.A. & White, N.J., 1989. Normal faulting in the upper continental crust: observations from regions of active extension, *J. struct. Geol.,* **11,** 15–36.

Kind, R. & Hanka, W., 1992. Erweitertes Angebot seismologischer Breitbanddaten am seismologischen Zentralobservatorium Gräfenberg (in German), *DGG Mitteilungen,* **1–2,** 58–61.

Koch, K., 1991a. Moment tensor inversion of local earthquake data—I Investigation of the method and its numerical stability with model calculations, *Geophys. J. Int.,* **106,** 305–319.

Koch, K., 1991b. Moment tensor inversion of local earthquake data—II. Application to aftershocks of the May 1980 Mammoth Lakes earthquakes, *Geophys. J. Int.,* **106,** 321–332.

Nábelek, J.L., 1984. Determination of earthquake source parameters from inversion of body waves, *PhD thesis,* MIT Cambridge, MA.

Müller, G., 1985. The reflectivity method: a tutorial, *J. Geophys.,* **58,** 153–174.

Patton, H.J., 1982. Measurements of Rayleigh-wave phase

velocities in Nevada: implications for explosion sources and the Massachusetts Mountain earthquake, *Bull. seism. Soc. Am.*, **72,** 1329–1349.

Paulssen, H., Dost, B. & van Eck, T., 1992. The Roermond earthquake of April 13, 1992; first interpretation of the NARS seismograms, *Geol. Mijnbouw*, **71,** 91–98.

Scherbaum, F., 1993. Modelling the Roermond earthquake of 1992 April 13 by stochastic simulation of its high frequency strong ground motion, *Geophys. J. Int.*, submitted.

Sipkin, S.A., 1982. Estimation of earthquake source parameters by the inversion of waveform data: synthetic waveforms, *Phys. Earth planet. Inter.*, **30,** 242–259.

Sipkin, S.A., 1986. Estimation of earthquake source parameters by the inversion of waveform data: global seismicity, 1981–1983, *Bull. seism. Soc. Am.*, **76,** 1515–1541.

Sipkin, S.A. & Needham, R.E., 1993. Moment-tensor solutions estimated using optimal filter theory: global seismicity, 1991, *Phys. Earth planet. Inter.*, **75,** 199–204.

Thio, H.K. & Kanamori, H., 1992. Moment tensor inversion in Southern California using surface waves recorded by TERRAscope (abstract), *EOS, Trans. Am. geophys. Un.*, **73**(43), 376.

Tichelaar, B.A. & Ruff, L.R., 1989. How good are our best models? Jackknifing, bootstrapping, and earthquake depth, *EOS, Trans. Am. geophys. Un.*, **70**(20), 593–606.

Wallace, T.C., Ammon, C., Lay, T., Ritsema, J. & Patton, H., 1992. Rapid source parameter retrieval at regional distance: a comparison of techniques (abstract), *EOS, Trans. Am. geophys. Un.*, **73**(43), 372.

Ward, S., 1980. Body wave calculation using moment tensor sources in spherically symmetric, inhomogeneous media, *Geophys. J. R. astr. Soc.*, **60,** 53–66.

Zijerveld, L., Stephenson, R., Cloetingh, S., Duin, E. & van den Berg, M.W., 1992. Subsidence analysis and modelling of the Roer Valley Graben (SE Netherlands), *Tectonophysics*, **208,** 159–171.